Design of a novel intermittent self-closing mechanism for a MACCEPA-based Series-Parallel Elastic Actuator (SPEA)

Mathijssen, Glenn; Furnemont, Raphaël; Brackx, Branko; Van Ham, Ronald; Lefeber, Dirk; Vanderborght, Bram

Published in:
Proceedings of the IEEE/RSJ International Conference on Intelligent Robots and Systems (IROS 2014)

DOI:
10.1109/IROS.2014.6942947

Publication date:
2014

License:
Unspecified

Document Version:
Accepted author manuscript

Design of a novel intermittent self-closing mechanism for a MACCEPA-based Series-Parallel Elastic Actuator (SPEA)

Glenn Mathijssen[1], Raphaël Furnémont, Branko Brackx, Ronald Van Ham, Dirk Lefeber and Bram Vanderborght

***Abstract*— High-performance actuators are required for numerous novel applications such as human-robot assistive devices. The torque-to-weight ratio and energy efficiency of current actuation technology is often too low, which limits the performance of novel robots. Therefore, we developed a Series-Parallel Elastic Actuator (SPEA) which enables variable recruitment of parallel springs and variable load cancellation. Finding suitable intermittent mechanisms for the SPEA is however still challenging. This paper reports on the innovative design of an intermittent self-closing mechanism for a MACCEPA-based SPEA that can deliver bi-directional output torque and variable stiffness, while minimizing friction levels. Experiments on a one-layer intermittent self-closing mechanism are conducted to validate the working principle and the proposed model. A demonstrator of the MACCEPA-based SPEA with intermittent self-closing mechanism is presented and the experiments validate the modeled output torque and lowered motor torque for different stiffness settings.**

I. INTRODUCTION

Research towards high-performance actuators is of high interest for the whole robotics community since this automatically leads to robots with improved performance [1], which are required for numerous novel applications such as human-robot assistive devices.

Apart from advantages such as safety and robustness for working in a dynamic environment by means of impedance control [2] [3], Series Elastic Actuators (SEA) [4] and Variable Stiffness Actuators (VSA) [5] [6] [7] have been introduced to improve the performance in comparison with stiff actuators by storing and releasing energy via the spring. A recent review can be found in [8] . Firstly, this can be useful for applications that require a high power burst (e.g. kicking, hammering, etc. [9]). Secondly, in cyclic applications a SEA can store energy in the spring during a period of negative power and release the energy during a period where power generation is required (e.g. ankle prosthesis, motions with periodical deceleration, etc. [10]). In both cases, the speed of the motor can be reduced [11], which means a reduction in required mechanical power and required overall energy per cycle. Although these characteristics are interesting for multiple applications [8], still numerous applications exist where the unavailability of high-performance actuators limits the development (e.g. exoskeletons, prosthetics, manipulators for human robot interaction etc.) [12].

The problem analysis presented in [13], concluded that a major remaining problem resides in the fact that for either a stiff actuator, a SEA or a VSA, the full output load always stresses the motor since motor and load are in series. This is indicated in Fig. 1 where the three linear schematics clarify that the output force is proportional to the force which loads the motor $F_{motor} = F_{output}$. Furthermore, a robotic joint typically operates at high torque and low speed, which is opposite to the nominal operation of an electric motor. Therefore, gear trains with high reduction ratios are required. The energy losses, however, increase with the number of stages and the weight increases with the maximum output torque. High torque electric motors are also heavy since the weight of electric motors is proportional to the maximum continuous output torque of the motor [14]. Furthermore, the quadrant of low speed and high torque is the most inefficient quadrant in the energy efficiency contour of electric motors. Therefore, electric motors in robotics often work significantly below their maximum energy efficiency since the iron losses are in quadratic relation with the current, which is in linear relation with the motor torque. In general, one could state that the low torque-to-weight ratio and low energy efficiency are mainly limiting the performance of current actuator technology driven by electric motors [13].

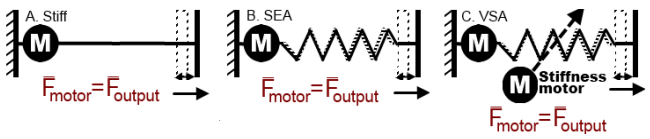

Fig. 1. The linear schematics of a stiff actuator, a SEA and a VSA clarify that the output force is proportional to the force which loads the motor $F_{motor} = F_{output}$.

In contrast to a SEA, a Parallel Elastic Actuator (PEA) has a spring in parallel to the motor and can provide load cancellation. If the stiffness of the PEA is well tuned, the parallel spring can deliver most of the required output torque while the motor should only deliver the difference [15]. Other authors also compared SEAs and PEAs [16]. One disadvantage of a PEA is that it limits movement dexterity since it is always engaged. Therefore, Haeffle et al. designed a clutchable PEA (cPEA) where the parallel spring can be connected or disconnected [17], and Au et al. implemented a uni-directional parallel spring in their ankle prosthesis [18].

*This work was supported in part by the ERC-grant SPEAR (no.337596)

All authors are with the Robotics & Multibody Mechanics Research Group (R&MM), Faculty of Mechanical Engineering, Vrije Universiteit Brussel, 1050 Elsene, Belgium `http://mech.vub.ac.be/robotics`

[1]Corresponding author: `Glenn.Mathijssen@vub.ac.be`

These solutions are, however, only binary solutions and thus still limited to specific applications, while most robots need to preform very versatile tasks.

The novel compliant actuation concept SPEA addresses these problems by variable recruitment of parallel elastic elements. The concept is introduced in [19] by means of a first demonstrator with mutilated gears as an intermittent mechanism. The experiments showed the feasibility of lowering the motor torque requirements and drastically increasing the energy efficiency. In this paper we present a novel intermittent self-closing mechanism, that solves the drawbacks of the previous design with mutilated gears. More specifically it allows for bi-directional output torque, reduced friction levels and has the potential of variable stiffness.

After a brief repetition of the general SPEA and schematics of the The Mechanically Adjustable Compliance and Controllable Equilibrium Position Actuator (MACCEPA), section II presents the concept of a MACCEPA-based SPEA. Section III presents the innovative model of the intermittent self-closing mechanism and validates its working principle. Section IV describes and validates the model of the input and output characteristics of the MACCEPA-based SPEA with intermittent self-closing mechanism. Section V presents the experimental results on a one-layer self-closing mechanism and on a four-layer MACCEPA-based SPEA demonstrator. Section VI concludes the paper.

II. CONCEPT OF A MACCEPA-BASED SPEA

As shown in the schematic in Fig. 2, the SPEA consists of one motor (solid black circular motor symbol) which can shift position (shaded motor symbols) to variably tension and lock each successive parallel spring. This variable recruitment results from multiple dephased intermittent mechanisms in parallel that position the motor from spring to spring, represented by the blue dotted rectangle. This allows to tension each parallel spring of the SPEA from unpretensioned to pretensioned phase (or vice versa) during the pretensioning phase. As a result, the motor of a SPEA with n springs is only loaded by the force of one spring of which the stiffness is n times lower than the stiffness of the spring in an equivalent SEA. In [19] we proved that as such, the motor torque is only a fraction of the output load.

The original MACCEPA design [5] is shown in Fig. 3.A. It consists of a motor, fixed to the ground link, which actuates a lever arm (red) of length B that rotates around the joint axis. A spring is connected to the lever arm and to the output link. The equilibrium position φ is the position where the actuator generates zero torque. The output torque T_{output} is a function of the deviation angle α. By increasing the pretension P of the spring with a second motor, the stiffness of the joint can be independently varied. Since only a single linear spring is required, the MACCEPA allows for a straight-forward non-complex design. Due to these virtues the MACCEPA is used in many applications (e.g. [5] [20]).

To design a MACCEPA-based SPEA, a novel altered MACCEPA is required that enables to disconnect the motor arm (red) from the spring when the motor arm angle $|\omega|$

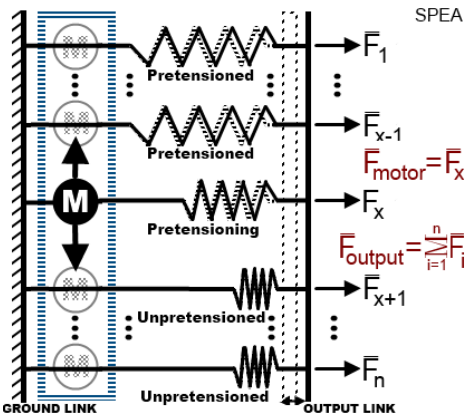

Fig. 2. The SPEA schematic shows that the output force equals the sum of the forces exerted by all springs, while the motor is only loaded by the force of the pretensioning spring.

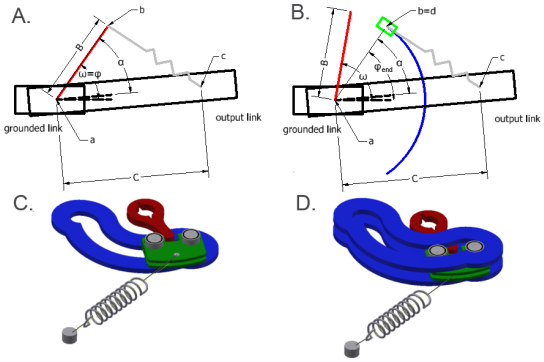

Fig. 3. A: the original MACCEPA schematic and nomenclature. B: schematic and nomenclature of the novel MACCEPA with guide (blue) and tensioner (green), which shows that the motor arm (red) disconnects from the spring at $|\varphi_{end}|$. C and D: Practical arrangement of motor arm, tensioner, guide and spring.

exceeds φ_{end}, and then locks the spring at φ_{end} as presented in Fig. 3.B. Henceforth, the motor arm angle is defined as ω and the equilibrium angle φ. As such, this results in an intermittent mechanism which can be expressed as (1).

$$\varphi = \begin{cases} \varphi_{end} & \omega > \varphi_{end} \\ \omega \quad if & |\omega| \leq \varphi_{end} \\ -\varphi_{end} & \omega < -\varphi_{end} \end{cases} \tag{1}$$

The intermittent MACCEPA mechanism is realized by means of a motor arm (red) that drives a tensioner (green), which is fixed to a spring and positioned between 2 guides (blue). This is shown in Fig. 3.C & D. When $\varphi = \omega$, the motor arm (red) drives the tensioner who's trajectory is defined by the model of the guide. Friction between the guide and the tensioner is minimized by using bearings as followers for the guide. The self-closing ends of the guides ensure that the lever arm automatically decouples from the tensioner at the end of the guide.

The idea for the MACCEPA-based SPEA is to stack multiple self-closing intermittent mechanisms, shown in Fig. 3.D, in parallel. The motor arms, which are fixed to the motor axis, are dephased with respect to each other. As such, a motor that continuously drives the motor axis can tension and

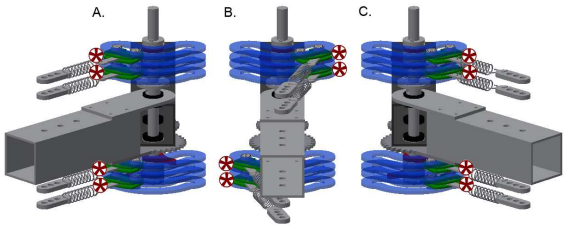

Fig. 4. By positioning the tensioners (indicated by the red stars), the equilibrium position of the MACCEPA-based SPEA can be altered. In A and C, the maximum equilibrium angle is achieved, while for B the equilibrium angle is 0°.

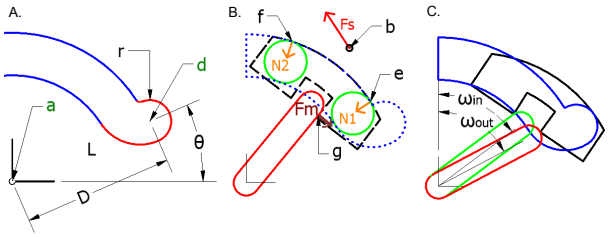

Fig. 5. A: the parameters that fully constrain the model of the guide. B: forces acting on the tensioner. C: illustration of the difference in motor arm angle ω when locking (ω_{in}) or unlocking (ω_{out}) the tensioner.

lock each of the parallel springs in succession. The stiffness of the actuator can be varied by changing the pretension of each of the parallel springs, similar the MACCEPA. The neutral position of the MACCEPA-based SPEA is obtained by positioning half of the parallel springs at φ_{end} and the other half at $-\varphi_{end}$, as shown in Fig. 4.B. The maximum equilibrium angle can be achieved by positioning all springs at φ_{end} or at $-\varphi_{end}$, as shown in Fig. 4.A & C.

III. MODEL OF THE INTERMITTENT SELF-CLOSING MECHANISM

The characteristics of the intermittent self-closing mechanism are determined by the model of the guide. The guide presented in this paper consists of 2 main sections as shown in Fig. 5.A:

- The middle section (blue): this geometry determines the extension of the spring, and as such it determines the output torque profile.
- Both outer sections (red): this geometry determines the range of equilibrium angles $[-\varphi_{end}, \varphi_{end}]$ and the range of output angles where the locking is guaranteed $[-\Psi_{unlock}, \Psi_{unlock}]$.

The geometry of the middle section of the guide is circular. As such, the mechanism is similar to a MACCEPA. The geometry of the end of the guide needs to be designed as such that the locking of the spring is guaranteed. Figure 5.A shows the parameters that fully constrain the model of the guide: D, Θ, R, and r.

The parameters R and r can be chosen first:

- *r*: is the radius of the bearing. The bearing should be chosen so that it does not fail due to the forces exerted on the tensioner by the spring.

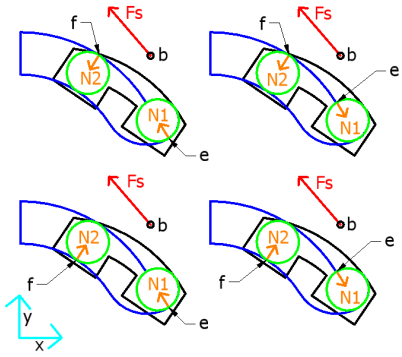

Fig. 6. The four different possible combinations of normal forces when the tensioner is locked. For a certain orientation and magnitude of the force of the spring F_s, only combination for which both normal forces are positive in the calculations is valid.

- *R*: in first approximation $R+r$ is equal to the motor arm length B. As such, R can be chosen to obtain a certain ratio C/B which determines a certain required stiffness profile, as was done for the standard MACCEPA in [5].

The two remaining parameters D and Θ are still undetermined. From Fig. 5.A one can see that D and Θ define the end of the guide. It should be verified for any combination of D and Θ, whether the motor angle at which the motor arm disconnects from the tensioner, ω_{out}, is greater than the motor angle at which the motor arm reconnects with the tensioner ω_{in}. This is indicated in Fig. 5.C.

In order to calculate the range of output angles where the locking is guaranteed $[-\psi_{unlock}, \psi_{unlock}]$, we assume the contact between the bearings and the guide to be frictionless. Since friction will only improve the locking, this assumption can be considered as a safety margin. As a result, the reaction forces between the bearings and the guide are normal to the guide. The free body diagram shown in Fig. 6 of the tensioner is considered which consists of 3 forces: the two reaction forces $\vec{N}_1$ and $\vec{N}_2$ between the bearings and the guide, and the force of the spring $\vec{F}_s$. The analysis of the locking is based on the static equilibrium of the tensioner (2) (moment equilibrium around the contact point of bearing 2 and the guide).

$$\begin{cases} F_{s,x} + 2N_{1,x} + 2N_{2,x} = 0 \\ F_{s,y} + 2N_{1,y} + 2N_{2,y} = 0 \\ \vec{fe} \times \vec{N_1} + \vec{fb} \times \vec{F_s} = \vec{0} \end{cases} \tag{2}$$

It is important to note that the factor 2 in (2) is a result of the fact that each tensioner is positioned between 2 guides. Furthermore, it is important to note that the geometry of the guide is included in (2) since the forces are projected in the XY frame. The projection of $\overline{F}_s$, for example, yields to (3).

$$\begin{aligned} F_{s,x} &= F_s(x_b(\varphi) - x_c(\Psi))/l \\ F_{s,y} &= F_s(y_b(\varphi) - y_c(\Psi))/l \end{aligned} \tag{3}$$

With $l = \sqrt{x_b(\varphi) - x_c(\Psi))^2 + (y_b(\varphi) - y_c(\Psi))^2}$ and F_s the amplitude of the force of the spring. As described before, the geometry parameters R, and r are fixed. If we now select a value for the Θ and D, the geometry is fully

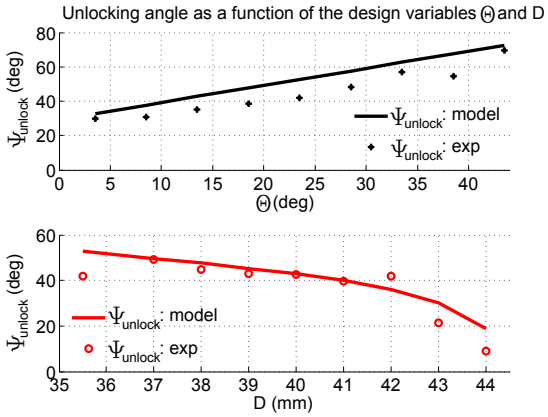

Fig. 8. The experiments of the locking region of 18 guides with different design variables Θ and D approximate the modeled locking region.

constraint. The following reasoning will then determine the locking range $[-\Psi_{unlock}, \Psi_{unlock}]$. Since the geometry is fixed, and since the reaction forces are normal to the guide, the orientation of $\vec{N}_1$ and $\vec{N}_2$ is known. As such, it is clear that (2) has 3 unknowns: the magnitude of the reaction forces N_1 and N_2, and the output angle of the link Ψ (which in turn determines $\vec{F}_s$ when the tensioner is locked). The static equilibrium of (2) can be solved since it consists of 3 equations and 3 unknowns. This calculation can be done for the 4 different combinations of contact points between the bearings and the guide, as illustrated in Fig. 6. The solution where both N_1 and N_2 are positive is the correct solution and thus corresponds to the correct configuration of contact points f and e. The value Ψ obtained by this correct solution, equals the unlocking angle Ψ_{unlock}. The locking region is therefore limited to output angles Ψ which are smaller than Ψ_{unlock}.

The design method described here above is experimentally validated and the results can be found in Fig. 8. The experiment consists of measuring the locking region of 18 guides with different Θ and D, produced by laser cutting. This was practically realized by increasing the output angle until the tensioner unlocked at Ψ_{unlock}. In total we tested the locking region of 9 guides with increasing Θ (from 3.5° to 43.5°.) and 9 guides with increasing D (from 34.5 mm to 44 mm). Each experimental data point in Fig. 8 is the average of 5 experiments on one of the 18 guides. The standard deviation is smaller than the marker size. The results indicate that for an increase in Θ, the locking region increases while the reverse is true for D. More important, however, is the fact that the measured Ψ_{unlock} clearly approximates the modeled values. As a result, the guides can be designed, with a locking region according to the requirements of a certain application, based on our model.

IV. MODEL OF INPUT AND OUTPUT CHARACTERISTICS OF THE MACCEPA-BASED SPEA WITH INTERMITTENT SELF-CLOSING MECHANISM

A. General equations

A MACCEPA-based SPEA with n self-closing mechanisms in parallel is considered. For each layer, an equilibrium angle φ_i and a deviation angle α_i are defined. It is important to note that due to (1), a specific motor angle ω corresponds to a certain set of φ_i's. This is due to the fact that at a certain motor angle ω, the tensioner of each layer will be in a specific position. Since the spring of each self-closing mechanism is connected to the output of the MACCEPA-based SPEA, the output angle Ψ_{spea} equals the output angle of each layer. This results in (4) for each of the n layers.

$$\psi_{spea} = \varphi_i + \alpha_i \tag{4}$$

Comparable to φ_i and α_i as defined for each layer, the MACCEPA-based SPEA itself is a compliant actuator as well and therefore an equilibrium angle φ_{spea} and deviation angle α_{spea} are defined and related according to (5)

$$\psi_{spea} = \varphi_{spea} + \alpha_{spea} \tag{5}$$

Logically, when the output torque T_{spea} is equal to 0, the equilibrium angle φ_{spea} is equal to the output angle Ψ_{spea}. As previously reasoned with regard to φ_i, the equilibrium angle φ_{spea} is dependent on the motor angle ω.

B. Motor and output torque of one layer

Apart from the pretension P and the geometrical constraints, the output torque of a standard MACCEPA is dependent on the deviation angle α. The equation for the output torque of the self-closing MACCEPA is similar to the one of the standard MACCEPA. The only difference is that for the self-closing MACCEPA, B (the distance between a and the contact point of the motor arm and the tensioner) is dependent on the equilibrium angle φ_i, since the spring is connected to the tensioner, which slightly moves relative to the motor arm. The details of this difference are out of the scope of this paper. The output torque generated by a certain layer T_i can be calculated according to (6):

$$T_i(\varphi_i, \alpha_i) = kB(\varphi_i)C\sin\alpha_i \left(1 + \frac{P + \mid B(\varphi_i = 0) - C \mid}{\sqrt{B(\varphi_i)^2 + C^2 - 2B(\varphi_i)C\cos\alpha_i}}\right) \tag{6}$$

Similar to the reasoning in section III, the motor torque T_{motor} of the MACCEPA-based SPEA can be calculated by solving the static equilibrium of the forces acting on the tensioner, as shown in Fig. 5.B. Additional to the forces $\vec{N}_1$, $\vec{N}_2$, $\vec{F}_s$ in Fig. 6, the force of the motor arm $\vec{F}_{motor}$ on the tensioner is also present in the free body diagram. Since the angles φ_i are determined for a certain ω, the spring force F_s is known as well. Therefore, the only unknowns are N_1, N_2 and F_{motor}, which can be determined by solving the system

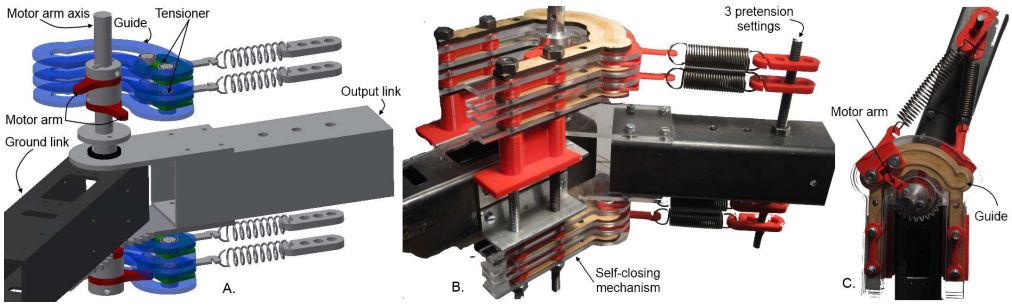

Fig. 7. A and B: 3D drawing and a picture of the MACCEPA-based SPEA with 4 layers. B: close-up on the tensioner and the guide.

of 3 equations (7) (moment equilibrium around the origin in point a):

$$\begin{cases} F_{motor\,x} + F_{sx} + 2N_{1x} + 2N_{2x} = 0 \\ F_{motor\,y} + F_{sy} + 2N_{1y} + 2N_{2y} = 0 \\ \vec{ae} \times \vec{N_1} + \vec{af} \times \vec{N_2} + \vec{ab} \times \vec{F_s} + \vec{ag} \times \vec{F_{motor}} = 0 \end{cases} \tag{7}$$

When F_{motor} of the lever arm is determined, T_m is determined by means of $\vec{T_{motor}} = \vec{ag} \times \vec{F_{motor}}$. One can note that $|\vec{ab} \times \vec{F_s}|$ is equal to (6).

C. Motor settings for a required output profile

The motor torque T_{motor} and motor angle ω can be calculated based on a required output torque T_{spea} and position Ψ_{spea}, which we will further refer to as T_{req} and Ψ_{req}.

Since the n layers actuate the output in parallel to each other, the output torque of the MACCEPA-based SPEA can be calculated as the sum of the output torque generated by each layer i, as depicted in (8):

$$T_{spea} = \sum_i T_i\left(\varphi_i, \alpha_i\right) \tag{8}$$

Based on (4) and (8), we can write (9):

$$\begin{aligned} \psi_{req} &= \varphi_i + \alpha_i \\ T_{req} &= \sum_i T_i\left(\varphi_i, \alpha_i\right) \end{aligned} \tag{9}$$

By iteratively solving equations (9) for φ_i and α_i, the required motor angle ω is known since a certain ω corresponds to a certain set of φ_i. By means of (7) the required motor torque T_{motor} can then be calculated.

V. EXPERIMENTAL RESULTS

The demonstrator presented in this section V consists of 4 parallel springs and thus 4 parallel self-closing MACCEPAs. The motor arms of each parallel self-closing MACCEPA are fixed to the same motor axis, and are dephased by approximately 90° (as can be seen in Fig. 7.A). The motor should be able to tension all 4 springs from $-\varphi_{end}$ to φ_{end} in 360° since otherwise the first motor arm will coincide with its tensioner after turning 360°. The range of equilibrium angles $[-\varphi_{end}, \varphi_{end}]$ of the demonstrator is therefore maximum $[-45°, 45°]$. As indicated in Fig. 7.B, the MACCEPA-based

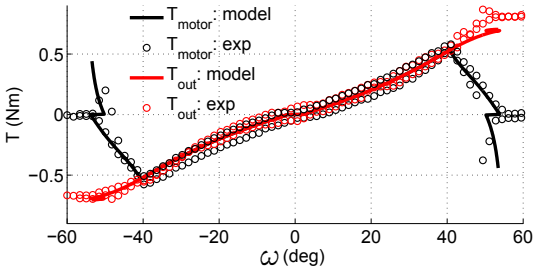

Fig. 10. The motor torque and output torque, of one layer, are similar in the central section of the guide and differ at the extremities where the tensioner is locked. The experiments clearly match the model.

SPEA has also the possibility of pretensioning the springs to change the stiffness of the actuator.

The demonstrator, shown in Fig. 7.A, consists of 4 springs with a stiffness k of 510 N/m. The distance from the motor axis to the connection of the springs to the output link, C is equal to 130 mm. The radius of the bearings r is 5 mm and R is 25 mm. Furthermore, the distance to the end of the guide D is 35.5 mm and the angle to the end of the guide Θ is 23.5°. These values were tuned according to the procedure described in section III to ensure the locking is guaranteed.

In order to validate the working principle of the MACCEPA-based SPEA and to validate the models of section IV, the motor torque and the output torque were measured and compared with the models. The main goal of these experiments is to show the lowered motor torque compared to the output torque and to validate the models. For this experiment, the output of the actuator is blocked at 0° and two force sensors (one at each side) measure the output torque generated by the output link of the MACCEPA-based SPEA. The motor angle ω was measured together with the motor torque T_{motor}, which was measured with a Messtechnic torque sensor.

The results of the experiments on 1 layer are presented in Fig. 10. The experiment was repeated 10 times, the average values are presented. The standard deviation is smaller than the marker size. It is clearly shown that the measurements match the model. T_{motor} and T_{out} are similar during the central section of the guide. This is due to the fact that the central section of the guide is modeled as a MACCEPA, and T_{motor} and T_{out} of a MACCEPA are similar. The experiments confirm that $|T_{motor}|$ decreases at the extremities of

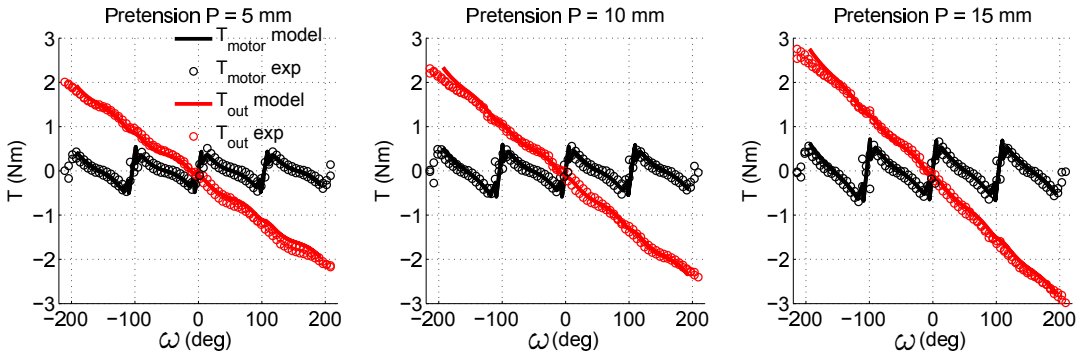

Fig. 9. T_{motor} is approximately 4 times lower than T_{out}. Increasing the pretension increases the stiffness and the maximum T_{out}.

the guide where the tensioner is locked. Fig. 10 also clearly shows that when $|\omega| \geq 55°$, the motor torque drops to zero while the output torque remains at its maximum.

Finally, the results of the experiments on the complete MACCEPA-based SPEA are presented in Fig. 9. The experiments are repeated for 5 mm, 10 mm and 15 mm pretension. The measurements clearly match the model and the standard deviation is smaller than the marker size. Furthermore, the motor torque is indeed lowered compared to the output torque. The increase in pretension by 10 mm changed the stiffness of the actuator by 32%.

VI. CONCLUSION

In this paper a novel MACCEPA-based Series-Parallel Elastic Actuator with a self-closing mechanism is presented, that consists of a guide and a tensioner. A model was proposed to guarantee a certain output angle range in which the tensioner is locked. The model is validated on 18 different guides. Furthermore, a model is presented to calculate the required motor action for a certain required output profile. The experiments on a one-layer self-closing MACCEPA, and the experiments on a 4 layer MACCEPA-based SPEA validated the model. Furthermore, the experiments proved the main virtues of this actuator, namely the lowered motor torque by recruitment of parallel springs, bi-directional force output and variable stiffness. Future work consists of producing metal guides and optimizing the size and weight of the actuator. The complexity of the SPEA increases indeed compared to VSAs. However, this becomes feasible due to the technological developments in the field of additive manufacturing techniques. Our study regarding the SPEA is an exploratory study towards innovative novel actuators for improved torque-to-weight ratios and energy efficiency.

REFERENCES

[1] H. Christensen, T. Batzinger, K. Bekris, K. Bohringer, J. Bordogna, G. Bradski, O. Brock, J. Burnstein, T. Fuhlbrigge, R. Eastman, *et al.*, "A roadmap for us robotics: From internet to robotics," *Computing Community Consortium and Computing Research Association, Washington DC (US)*, 2009.

[2] A. Bicchi, G. Tonietti, M. Bavaro, and M. Piccigallo, "Variable stiffness actuators for fast and safe motion control," *International Journal of Robotics Research*, pp. 527–536, 2005.

[3] M. Zinn, O. Khatib, B. Roth, and J. Salisbury, "Playing it safe [human-friendly robots]," *IEEE Robotics Automation Magazine*, vol. 11, no. 2, pp. 12–21, 2004.

[4] G. A. Pratt and M. M. Williamson, "Series elastic actuators," in *IEEE/RSJ International Conference on Intelligent Robots and Systems (IROS)*, vol. 1, 1995, pp. 399–406.

[5] R. Van Ham, B. Vanderborght, M. Van Damme, B. Verrelst, and D. Lefeber, "Maccepa, the mechanically adjustable compliance and controllable equilibrium position actuator: Design and implementation in a biped robot," *Robotics and Autonomous Systems*, vol. 55, no. 10, pp. 761–768, October 2007.

[6] S. Wolf, O. Eiberger, and G. Hirzinger, "The dlr fsj: Energy based design of a variable stiffness joints," in *IEEE International Conference on Robotics and Automation (ICRA)*, 2011, pp. 5082–5089.

[7] A. Jafari, N. Tsagarakis, and D. G. Caldwell, "Awas-ii: A new actuator with adjustable stiffness based on the novel principle of adaptable pivot point and variable lever ratio," in *IEEE International Conference on Robotics and Automation (ICRA)*, 2011, pp. 4638–4643.

[8] B. Vanderborght, A. Albu-Schaeffer, A. Bicchi, E. Burdet, D. Caldwell, R. Carloni, M. Catalano, O. Eiberger, W. Friedl, G. Ganesh, *et al.*, "Variable impedance actuators: A review," *Robotics and Autonomous Systems*, vol. 61, no. 12, pp. 1601–1614, 2013.

[9] M. Garabini, A. Passaglia, F. Belo, P. Salaris, and A. Bicchi, "Optimality principles in stiffness control: The vsa kick," in *IEEE International Conference on Robotics and Automation (ICRA)*, 2012, pp. 3341–3346.

[10] J. Pons, "Rehabilitation exoskeletal robotics," *IEEE Engineering in Medicine and Biology Magazine*, vol. 29, no. 3, pp. 57–63, May 2010.

[11] T. G. Sugar and M. Holgate, "Understanding speed and force ratios for compliant mechanisms," in *Advances in Mechanisms, Robotics and Design Education and Research*. Springer, 2013, pp. 117–129.

[12] D. Tesar, "Overview of the long term objectives of the journal actuators," *Actuators*, vol. 1, no. 1, pp. 1–11, 2012. [Online]. Available: http://www.mdpi.com/2076-0825/1/1/1

[13] G. Mathijssen, P. Cherelle, D. Lefeber, and B. Vanderborght, "Concept of a series-parallel elastic actuator for a powered transtibial prosthesis," *Actuators*, vol. 2, no. 3, pp. 59–73, 2013.

[14] J. H. Marden, "Scaling of maximum net force output by motors used for locomotion," *Journal of Experimental Biology*, vol. 208, no. 9, pp. 1653–1664, 2005.

[15] J. Herder, "Design of spring force compensation systems," *Mechanism and machine theory*, vol. 33, no. 1, pp. 151–161, 1998.

[16] M. Grimmer, M. Eslamy, S. Gliech, and A. Seyfarth, "A comparison of parallel-and series elastic elements in an actuator for mimicking human ankle joint in walking and running," in *IEEE International Conference on Robotics and Automation (ICRA)*, 2012, pp. 2463–2470.

[17] D. F. B. Haeufle, M. D. Taylor, S. Schmitt, and H. Geyer, "A clutched parallel elastic actuator concept: Towards energy efficient powered legs in prosthetics and robotics," in *IEEE RAS EMBS International Conference 4th on Biomedical Robotics and Biomechatronics (BioRob)*, 2012, pp. 1614–1619.

[18] S. K. Au, J. Weber, and H. Herr, "Powered ankle–foot prosthesis improves walking metabolic economy," *IEEE Transactions on Robotics*, vol. 25, no. 1, pp. 51–66, 2009.

[19] G. Mathijssen, D. Lefeber, and B. Vanderborght, "Variable recruitment of parallel elastic elements: Series-parallel elastic actuators (spea) with dephased mutilated gears," *IEEE Transactions on Mechatronics*, 2014 (in press), (Accepted 3 February 2013).

[20] P. Cherelle, V. Grosu, A. Matthys, B. Vanderborght, and D. Lefeber,

"Design and validation of the ankle mimicking prosthetic (amp-) foot 2.0," *Neural Systems and Rehabilitation Engineering, IEEE Transactions on*, vol. 22, no. 1, pp. 138–148, Jan 2014.